Acta Cryst. (1995). B**51**, 559–570

Bond Lengths, and Beyond

BY RICCARDO DESTRO AND FELICITA MERATI

Dipartimento di Chimica Fisica ed Elettrochimica, e Centro CNR, via Golgi 19, 20133 *Milano, Italy*

(*Received* 5 *March* 1995; *accepted* 10 *April* 1995)

Abstract

The degree of precision and accuracy in molecular geometry attainable with modern X-ray diffraction and cryogenic techniques is documented by presenting the results of a low-temperature study of *syn*-1,6:8,13 biscarbonyl[14]annulene, tricyclo[8.4.1.1^{3,8}]hexadeca-2,4,6,8,10,12,14-heptaene-15,16-dione. Intensity data up to $\sin\theta/\lambda = 1.14$ Å^{-1} have been measured from a spherical crystal at $T = 19$ K. Their multipolar analysis, up to the octopole level for C and O atoms, and to quadrupoles for anisotropically described H atoms, has led to precisions in the coordinates of the heavy atoms which are better than 0.0004 Å. Root mean square (r.m.s.) amplitudes of vibration for C and O atoms have been determined to a precision of *ca* 0.0006 Å. Based on the least-squares σ's, uncertainties for the C—C and C—O bond lengths are 0.0005 Å, and those of the C—H bond distances 0.006–0.007 Å. The topological properties of the experimentally derived charge density of the annulene molecule in the crystal have been determined by evaluating the location and nature of its critical points (points where $\nabla\rho = 0$). Contour maps of ρ_{exp} and its negative Laplacian ($-\nabla^2\rho_{exp}$) are presented. The occurrence of a bond critical point midway between the two C atoms of the carbonyl bridges seems to indicate the existence of a chemically unexpected weak bond between the two C atoms.

1. Introduction

The results of an X-ray structure analysis are usually discussed by comparing the obtained geometry with a set of paradigmatic structural dimensions. For such a comparison to be meaningful, statistical significance tests must be used, as first shown 45 years ago by Cruickshank (1949), in a paper on the accuracy of electron-density maps. The author illustrated his proposed methods by a detailed examination of the dibenzyl structure, and concluded his study by stating that 'the standard deviations of random errors in any direction in the dibenzyl peak positions... are 0.0080 Å for three-dimensional syntheses, and 0.0167 Å for two-dimensional syntheses'. He also suggested that 'random errors of this magnitude may be typical of a large class of organic compounds'. Actually, a better precision could in favorable circumstances be obtained in those days, as in the projection study of salicylic acid, for which Cochran (1953) claimed that 'bond lengths and the charge distribution... have been measured with standard deviations of less than 0.01 Å and 0.1 e Å^{-2}, respectively'. A remarkable feature of this latter work is the reported attempt to allow for the effects of bonding in the calculation of structure factors, although the departure from spherical symmetry of covalently bonded atoms had been found to be, in Cochran's words, unexpectedly small. As a matter of fact, the contribution of an idealized redistribution of electrons in salicylic acid was effective in reducing R (from 0.058 to 0.041), but had no consequences on the experimental molecular geometry.

When, some years later, least-squares procedures replaced Fourier methods for the determination of refined positional parameters, estimates of errors for the charge density were no longer evaluated in studies devoted to the assessment of precise geometries. However, it remained obviously true that precision and accuracy in bond lengths and angles strictly depend on random and systematic errors in electron density (through its Fourier transform) measurements and calculations. As for investigations with intensities measured by photographic methods, among the best results were those reported by Marsh (1958) for glycine. At the end of a least-squares refinement based on an exceptionally extensive data set (all the reflections within the molybdenum sphere had been covered), for this amino acid limits of errors of *ca* 0.005 Å in the apparent bond distances and 0.3° in the bond angles were estimated. A further reduction of these limits, typically by a factor of 2–3, has been subsequently achieved with the use of automatic diffractometers equipped with electronically controlled counting devices.

Where are we now? Particularly for studies of molecular crystals, recent improvements in precision and accuracy have been obtained thanks to (1) the use of cryostats operating at temperatures below 30 K, and (2) the multipolar analysis of the diffracted intensity data. Indeed, new types of low-temperature equipments, based on commercially available closed-cycle helium refrigerators, have been successfully adapted to automatic X-ray diffractometers (see the contribution of F. K. Larsen in this same issue for more details). The well known advantages of data collection at low temperature – such as an increase in the number of significant high-order data, a reduction of molecular vibrations, so that complex models for the thermal motion can be avoided,

ISSN 0108-7681

Table 1. *List of compounds under study in Milano, with data collected at* $T \leq 30$ K

Compound	Acronym	Formula
Glycine	(GLY)	$C_2H_5NO_2$
L-Alanine	(LALA)	$C_3H_7NO_2$
1-Methyluracil	(MUR)	$C_5H_6N_2O_2$
Bis(dimethylamino)squaraine	(BDS)	$C_8H_{12}N_2O_2$
syn-Biscarbonyl[14]annulene	(BCA)	$C_{16}H_{10}O_2$
Citrinin	(CITR)	$C_{13}H_{14}O_5$
N—Cl derivative of benzamidine	(CL-BA)	$C_{13}H_{10}N_2FCl$
LRB/081	(LRB)	$C_{30}H_{30}N_6O_3S$
Pyrope*	(PYR)	$Mg_3Al_2Si_3O_{12}$

* Data collection performed at 30 K, to match the temperature of a neutron study (Artioli, 1994). Data of all the other crystals were measured at lower temperatures.

and a substantial decrease of thermal diffuse scattering – can all be obtained with only moderate effort. In our experience, once this new type of cryostat has been adequately mounted and centered on the diffractometer, its operation is less demanding than that of a gas-stream cooling apparatus. In particular, diffraction experiments lasting several weeks pose no serious problems, and relatively large crystal structures can be investigated.

Table 1 lists the compounds under study in our laboratory, for which X-ray data have been collected at $T \leq 30$ K: they range from the simplest of all amino acids, with five non-H atoms only, to a drug, a receptor antagonist of angiotensin II, with 40 non-H atoms and 30 H atoms per molecule. With the exception of pyrope, the substances in Table 1 all form molecular crystals, and hence are representative of the type of specimen that mostly benefits from a low-temperature investigation. Indeed, as shown in Table 2, even in the less favorable case the number of unobserved intensities ($I < 0$) does not exceed 10% of the total independent data, which amount, for $2\theta_{Mo} = 109°$, to more than five times those within the Cu sphere. Such a large number of high-order reflections implies that positional and atomic displacement parameters are determined with exceptional and unprecedented precision. Furthermore, if an electron population analysis of the X-ray diffraction data with a pseudoatom model (Stewart, 1976) is performed, this process will occur under optimal experimental conditions, since deconvolution of the electron distribution from its thermal motion can be safely assumed.

We have recently shown (Destro, Bianchi, Gatti & Merati, 1991; Destro & Merati, 1993) that by using such an aspherical-atom formalism, reliable and detailed representations of the *total* experimental charge density are obtained. Suitable descriptors of many relevant features of this electron distribution are its properties at the bond critical points, whose evaluation following Bader's approach has been described in a recent issue of the Transactions of the ACA (Bader, 1990*b*). It is this not-yet common characterization of a crystal structure by the topological analysis of ρ_{exp} that is meant by the word 'Beyond' in the title of the present paper.

Table 2. *Measurement of X-ray diffraction data for the molecular crystals of Table* 1: *general conditions and number of intensities*

Data collection
- Mo $K\alpha$ radiation (graphite monochromated)
- $(\sin\theta/\lambda)_{max} \approx 1.14$ ($2\theta_{Mo} = 109°$)
- $16 \leq T \leq 23$ K

Intensities

Crystal	Measured	Independent	Unobserved
GLY	10835	3822	33
LALA	8966	2535	16
MUR	20436	3568	224
BDS*	12967	5160	516
	24625	5163	402
BCA	12149	7350	22
CITR	36550	7954	260
CL-BA	27661	10130	68
LRB†	51365	14699	886

* Data of BDS were collected from two samples, obtained by different crystallization procedures.
† For this crystal $(2\theta_{Mo})_{max} = 75°$.

To illustrate all these recent developments in X-ray structural analysis, we present here some relevant features and results of the low-temperature study of *syn*-1,6:8,13-biscarbonyl[14]annulene (BCA, alternatively cited in the literature as 15,16-dioxo-*syn*-1,6:8,13-bismethano[14]annulene). This arene was first synthesized by Vogel and coworkers (Balci, Schalenbach & Vogel, 1981), and the experimental geometry derived from a room-temperature investigation has been published (Destro & Simonetta, 1977).

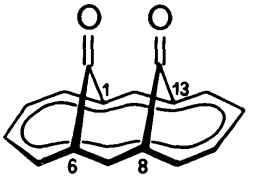

BCA

2. Experimental

2.1. *Data collection*

All diffraction data were obtained from the same crystal, ground to a sphere of approximate radius 0.17 mm and mounted on a four-circle diffractometer equipped with a local version of the Samson low-temperature apparatus (Samson, Goldish & Dick, 1980). Most of the relevant features, operative conditions and performances of the Milano instrument have been described within a report on the experimental determination of scan-truncation losses (Destro, 1988). The results of that study were based on accurate profile measurements, 649 in number, originating from the same BCA crystal we are dealing with here. Indeed, a detailed account was also given in that paper of an extensive data

set (about 12000 measurements), 'to be used for subsequent refinement of positional and thermal parameters of BCA'. For that set of data, slightly modified later (see §2.2), we add here some experimental features previously not reported:

(1) Three subsets were actually collected, with warming to room temperature in between. After the measurement of the 3326 intensities of the first subset (all within $2\theta_{Mo} = 55°$, with repeated monitoring of the strongest reflections at different tube settings), substantial changes to the instrument were made, such as replacement of the X-ray generator and the scintillation crystal of NaI(Tl) in the detector. Furthermore, modifications to the cryostat were developed and implemented after the measurements of each subset, especially to improve mechanical stability. As a result, the collection of the third portion of data occurred almost 2 years after that of the first. On the other hand, air and thermal stability (up to 773 K) is one of the outstanding chemical features of BCA (Balci, Schalenbach & Vogel, 1981; Vogel *et al.*, 1984): it is for this reason that the crystal employed for this study is still the reference sample for diffraction equipment in our laboratory.

(2) Temperature fluctuations during each subset collection never exceeded 2 K around the mean value. However, each cryostat arrangement corresponded to a different average temperature, namely 16.5, 21 and 22 K for the three portions of the data set, respectively. Further measurements (see below) were made at *ca* 17 K. We can reasonably assume 19 K as the average temperature of the experiment.

(3) Repeated measurements of cell dimensions, particularly before and after each set of intensity measurements, were performed. A total of 182 reflections were accurately centered, 90 at 16–17 K and 92 at 21–22 K. By the fitting of their $\sin^2\theta$ values, the following cell parameters were obtained: $a = 9.0480(9)$, $b = 12.6658(13)$, $c = 9.6516(8)$ Å, and $\beta = 94.344(7)°$; derived quantities are $V = 1102.9(2)$ Å^3 and $D_x = 1.411$ Mg m^{-3} (with $Z = 4$ in the monoclinic space group $P2_1/n$, formula weight for $C_{16}H_{10}O_2 = 234.26$). Unit-cell dimensions do not differ significantly from those obtained at 16(1) K, the temperature of the 649 profile measurements (Destro, 1988).

2.2. *Correction of the data*

The behavior of three standard reflections (375, $21\bar{8}$ and $5\bar{6}\bar{2}$) was periodically monitored during each of the three portions of the data collection. Within statistical uncertainty, the three standards behaved in a similar manner: a decrease in intensity during the first two subset measurements, and fluctuations never exceeding 1 e.s.d. during the third group of measurements. A linear decay, up to 1.5% over the 110 h of exposure to X-ray of the first subset, appeared adequate to represent the instability of its 3326 reflections, which were accordingly scaled. For the second subset two straight lines were obtained from a least-squares treatment of the standard intensities: one reproduced the behavior during the first 50 h, with a maximum decrease of 2.5%, and the second a further decrease of about the same amount during the following period of 170 h of exposure to X-rays. No decay correction was required by the data of the third subset, whose collection implied a total exposure of *ca* 95 h. Besides those for decay, Lorentz and polarization effects, no correction was deemed necessary for absorption, which was presumably negligible ($\mu = 0.086$ mm^{-1}). In view of the spherical shape of the crystal specimen, the beam-inhomogeneity, that had been previously mapped with a procedure similar to that described by Harkema, Dam, van Hummel & Reuvers (1980), was not taken into account. Rather, scan-truncation effects were corrected for, following the procedure developed by Destro & Marsh (1987, 1993; DM) and already applied to the 23 K data of L-alanine (Destro, Marsh & Bianchi, 1988). A beneficial side-effect of the DM procedure is an appreciable improvement of the precision of the net intensities, particularly for the weaker reflections, due to the replacement of individual values of the apparent background by inherent ('true') background values accurately measured. A detailed description of this and all other stages of the experimental determination of scan-truncation losses has been reported, for the specific case of the BCA crystal, in the already mentioned paper by Destro (1988).

Some tens of reflections were remeasured during the course of the structure refinement, since data analysis had indicated their ΔF's as anomalous, presumably affected by some sort of systematic error not yet accounted for. In a few cases the profile analysis indicated the presence of spikes, but most profiles showed a regular shape. Yet, when measured at different ψ values, net intensities were significantly different, thus revealing the phenomena of multiple reflections in the original measures. All these intensities were given revised values before the final multipole refinement cycles.

Each intensity was assigned a variance $\sigma^2(I)$ based on counting statistics plus an additional term $(0.015S)^2$, where S is the scan count. Weighted averaging of the 2684 reflections, mostly Cu-sphere data, common to two or more subsets ($R_{int} = 0.017$), led to a final set of 7350 independent intensities, of which only 22 had a negative value and were excluded from the final least-squares refinement.

2.3. *Refinement*

A preliminary least-squares refinement with the conventional spherical atom model led to the determination of the scale factor required to place the observed intensities of BCA on an approximately absolute basis. Such intensities were then analyzed with a number of different multipole models; we describe two of them, ($M1$) and ($M2$), here.

($M1$) According to the aspherical-atom formalism proposed by Stewart (1976), the one-electron density function is represented by an expansion in terms of rigid pseudoatoms, each formed by a core invariant part and a deformable valence part. Spherical surface harmonics (multipoles) are employed to describe the directional properties of the deformable part. Our model consisted of two monopole, three dipole, five quadrupole and seven octopole functions for each C and O atom. The generalized scattering factors (GSF) for the two monopoles of both atomic species were computed from the Hartree–Fock atomic functions tabulated by Clementi (1965). Electron population parameters of inner monopoles were constrained to be equal for all 18 non-H atoms. Single exponentials, $r^n \exp(-\alpha r)$, were adopted as radial functions for the higher multipoles, with $n = 2, 2, 3$ for dipole, quadrupole and octopole, respectively; the α values were the so-called standard molecular exponents (Hehre, Stewart & Pople, 1969). In the course of the refinement the H atoms were polarized in the direction of the C atom to which they were bonded. GSF's, including monopole and dipole terms, were initially assigned to each H atom and the corresponding curves were taken from the H_2 molecule (Stewart, Bentley & Goodman, 1975). In the final stages of the refinement the positional parameters of the H atoms were kept fixed, and these atoms too were described with multipoles up to the quadrupole level. For all three poles of the H pseudoatoms the radial functions were again single exponentials, with $n = 0, 1$ and 2 for monopole, dipole and quadrupole, respectively, and the α value was 2.48 bohr^{-1}.

The motions of all atoms were described by anisotropic displacement parameters (a.d.p.). The a.d.p.'s of C and O atoms were variable, and determined in the usual way by the least-squares process, while those of the H atoms were kept fixed at values calculated by first fitting **TLS** tensors to the complete molecule, then adding to the U_{ij}'s from the rigid-body motion contributions of 0.0065 Å^2 for a C—H stretch, 0.0145 Å^2 for in-plane bending and 0.0240 Å^2 for out-of-plane bending of each C—H bond (Hirshfeld, 1990). (These are rough guesses for the internal C—H vibrations, transferred from a normal-coordinate calculation for anthracene; the in-plane direction for each C—H is defined quite arbitrarily to contain one of the adjacent C—C bonds.) An isotropic extinction parameter, of type I and Lorentzian distribution (in the formalism of Becker & Coppens, 1974) completed the model, whose 542 variables therefore included 162 positional and displacement parameters for the 18 non-H atoms and 379 electron population parameters for the poles of various order for all 28 atoms in the asymmetric unit.

($M2$) An extension of ($M1$), to include a further six variables: a radial scaling parameter κ, to shape the outer shell monopoles, and the exponential parameter α, both constrained to be the same for all 16 C atoms; a similar pair for the O atoms and two α's for the H atoms, one (α_0) for the radial function of the monopole, and the other (α_H) for dipole and quadrupole functions. This assignment of radial parameters as variables closely parallels that adopted by Stewart (1991) for the analysis of imidazole and 9-methyladenine data.

All refinements were carried out using the *VALRAY* set of programs (Stewart & Spackman, 1983). We recall here that in Stewart's (1976) approach, as implemented in *VALRAY*, the scale factor is not included among the refinable parameters of multipole models; rather, it is estimated from the sum of the monopole populations divided by $F(000)$, the latter quantity being equal to 488 for BCA.

The quantity minimized in the least-squares calculations was $\varepsilon = \sum w(F_0^2 - k^2F_c^2)^2$, based on the 7328 reflections with $I > 0$ and with weights $w = \sigma^{-2}(F_0^2)$. For both models, convergence was assumed when the absolute value of the relative variation of ε in two subsequent cycles became $< 10^{-6}$. Full second derivatives were included in the least-squares matrix of the last cycle, to determine (through the evaluation of the correct Hessian of ε) that we were at a true minimum. Furthermore, the inverse Hessian elements could be used to estimate the variances of all properties of interest based on the GSF expansion.

3. Results and discussion

As shown by the summaries of Table 3, inclusion of radial parameters among the variables makes ($M2$) more adequate than ($M1$), with a significant decrease of all R indices and an even more evident improvement of the goodness-of-fit. Of particular relevance (see bottom of Table 3) is the better fit of ($M2$) to the experiment for reflections with $\sin\theta/\lambda \leq 0.65$, that is for the data which carry most of the information on valence electrons (Stewart, 1968). There is instead virtual identity of results from the two refinements for the 4806 data beyond the Cu-sphere, hence virtual identity in O and C atomic positions and mean square amplitudes of vibration.

There are 23 correlation coefficients greater than 0.707 (in absolute value) at the end of refinement ($M1$), none involving parameters of the H pseudoatoms. The largest six, in the range 0.84–0.86, are those of the dipole populations with the corresponding positional parameters for the two O atoms; all six decrease below 0.76 in refinement ($M2$), where only ten correlation factors involving parameters of the heavy atoms are above the same threshold value of $1/2^{1/2}$. The largest correlation coefficient for ($M2$), 0.84, occurs between the radial scaling parameter κ of the C atoms and the core monopole population, constrained to be the same for all 18 non-H atoms. On the other hand, the correlation matrix of refinement ($M2$) shows 23 coefficients > 0.707

Table 3. *Refinements of the observed intensities of BCA at* 19 K *with two multipole models*

	Model (*M*1)	Model (*M*2)
No. of observations	7328	7328
No. of parameters	542	548
Scale factor	1.0160 (13)	1.0044 (25)
Extinction coefficient*	0.290 (12)	0.224 (14)
Radial parameters†		
O atoms:		
κ	1.000	0.9945 (17)
α	4.50	4.05 (12)
C atoms:		
κ	1.000	1.0030 (19)
α	3.44	2.98 (2)
H atoms:		
α_0	2.48	2.40 (2)
α_H	2.48	3.03 (12)
$\varepsilon = \sum w\Delta^2$	10829.8	9491.8
CRIT‡	2.22×10^{-7}	9.55×10^{-7}
$R(F)$	0.0235	0.0228
$wR(F)$§	0.0180	0.0169
$R(F^2)$	0.0293	0.0273
$wR(F^2)$	0.0350	0.0327
Goodness-of-fit	1.2633	1.1832
Max. Δ/σ	0.0006	0.0024
Average Δ/σ	< 0.0001	0.0003
For the 2522 reflections within the Cu sphere		
$R(F)$	0.0134	0.0120
$wR(F)$§	0.0124	0.0105
$R(F^2)$	0.0160	0.0128
$wR(F^2)$	0.0240	0.0201

* In units of 10^{-4} (rad)^2.

† Kept fixed at the standard molecular values in model (*M*1); α's in bohr^{-1}.

‡ CRIT= $|\Delta\varepsilon|/\varepsilon_n$, where $\Delta\varepsilon = \varepsilon_n - \varepsilon_{n-1}$, and n is the cycle number.

§ This weighted R has been computed with $w = 4F_0^2/\sigma^2(F_0^2)$.

Table 4. *Final coordinates,* U_{eq}* *values* (Å^2) *and electron counts for BCA at* 19 K

	x	y	z	U_{eq}	Electrons
C1	0.61395 (4)	0.00201 (2)	0.28231 (3)	0.00442 (7)	6.06 (2)
C2	0.71684 (4)	−0.07168 (3)	0.23586 (4)	0.00597 (8)	6.12 (3)
C3	0.81064 (4)	−0.05134 (3)	0.13087 (4)	0.00640 (8)	6.06 (3)
C4	0.80002 (4)	0.02964 (3)	0.02789 (4)	0.00656 (8)	6.06 (3)
C5	0.69696 (4)	0.11108 (3)	0.00772 (4)	0.00595 (8)	6.08 (3)
C6	0.60292 (4)	0.14651 (2)	0.10869 (3)	0.00461 (7)	6.06 (2)
C7	0.46478 (4)	0.19535 (2)	0.08064 (3)	0.00516 (7)	6.03 (3)
C8	0.35848 (4)	0.19868 (2)	0.17919 (3)	0.00451 (7)	6.06 (2)
C9	0.20521 (4)	0.21658 (2)	0.14849 (3)	0.00537 (7)	6.07 (3)
C10	0.09310 (4)	0.17766 (3)	0.22605 (4)	0.00606 (8)	6.05 (3)
C11	0.09820 (4)	0.09437 (3)	0.32558 (4)	0.00640 (8)	6.09 (3)
C12	0.21682 (4)	0.02904 (3)	0.36884 (3)	0.00605 (8)	6.07 (3)
C13	0.36660 (4)	0.05165 (2)	0.34834 (3)	0.00461 (7)	6.08 (2)
C14	0.47916 (4)	−0.02297 (3)	0.33672 (3)	0.00505 (7)	6.05 (3)
C15	0.65560 (3)	0.11303 (2)	0.25199 (3)	0.00403 (7)	6.06 (2)
C16	0.39596 (3)	0.16579 (2)	0.32572 (3)	0.00417 (7)	6.06 (2)
O1	0.73752 (4)	0.16590 (3)	0.33015 (4)	0.00626 (8)	8.08 (3)
O2	0.43593 (4)	0.22648 (3)	0.41888 (4)	0.00641 (8)	8.06 (2)
H2	0.7164 (7)	−0.1508 (6)	0.2791 (7)	0.02275	0.83 (2)
H3	0.8911 (8)	−0.1129 (6)	0.1132 (7)	0.02319	0.86 (2)
H4	0.8735 (7)	0.0175 (5)	−0.0540 (7)	0.02360	0.90 (2)
H5	0.6844 (7)	0.1482 (5)	−0.0943 (7)	0.02291	0.91 (2)
H7	0.4308 (7)	0.2181 (5)	−0.0266 (7)	0.02150	0.87 (2)
H9	0.1736 (7)	0.2597 (5)	0.0523 (7)	0.02202	0.87 (2)
H10	−0.0200 (7)	0.2046 (5)	0.1942 (7)	0.02242	0.91 (2)
H11	−0.0082 (7)	0.0715 (5)	0.3582 (7)	0.02313	0.91 (2)
H12	0.1920 (7)	−0.0456 (6)	0.4177 (7)	0.02291	0.88 (2)
H14	0.4547 (7)	−0.1058 (5)	0.3555 (7)	0.02186	0.87 (2)

* $U_{eq} = 1/3(U_{11} + U_{22} + U_{33})$; e.s.d.'s were taken equal to: $\{1/6[\sigma^2(U_{11}) + \sigma^2(U_{22}) + \sigma^2(U_{33})]\}^{1/2}$ (Schomaker & Marsh, 1983).

between H parameters; all but two imply the exponential parameters α_0 and α_H and the largest does not exceed 0.83. We may conclude that the size of the data set for BCA at 19 K is such as to make correlation problems not too severe for these two multipole models. A detailed comparison between (*M*1) and (*M*2) is deferred to a forthcoming paper, where other descriptions, both spherical and multipolar, of BCA will also be discussed. Here we consider (*M*2) as our reference model for the crystal under study.

Final values for the position parameters are given in Table 4; the e.s.d.'s for the coordinates of the H atoms are those derived from the last least-squares cycle which included such parameters in the refinement. Anisotropic atomic displacement parameters have been deposited as supplemenary materials,* while equivalent U's are included in Table 4. It is seen that the number and quality of our experimental data, as measured at 19 K and analyzed by a multipole model, lead to the following:

(*a*) The coordinates of the non-H atoms are determined to a precision of 0.00025–0.00040 Å, while those of the H atoms to a precision of 0.0060–0.0075 Å.

(*b*) r.m.s. amplitudes of vibration for C and O atoms are determined to a precision of *ca* 0.0006 Å, which is significantly less than 1% of the root mean square amplitudes themselves.

The populations of the monopoles are listed in Table 4 as total electron counts, those of higher-order poles are among the deposited material. The electron population for the dipole terms is rather small for the 14 C atoms of the annulene perimeter, but appreciable for the four atoms of the two carbonyl groups. The quadrupole contribution is large for all 18 non-H atoms, smaller but definitely significant for the 10 H atoms. Octopoles are highly populated in all 16 C atoms, but much less, as expected, in the terminally bonded O atoms. Following Stewart's (1972) procedure, electronic parameters for monopoles and dipoles have been used to evaluate the molecular dipole moment of BCA in the crystal, yielding $|\mu| = 6.9$ D. Although accompanied by a rather large e.s.d. of 1.0 D, the value of μ derived from our experiment is certainly realistic, as shown by Spackman (1992) in his review on molecular electric moments from X-ray diffraction data.

* Lists of observed and calculated structure factors, anisotropic displacement parameters and electron populations for the various poles of the pseudoatoms, together with tables of all torsion angles, the least-squares planes of interest, the results of the rigid-bond test, and those for three different models of the rigid-body motion analysis have been deposited with the IUCr (Reference: HR0026). Copies may be obtained through The Managing Editor, International Union of Crystallography, 5 Abbey Square, Chester CH1 2HU, England.

Table 5. *Results of the rigid-body motion analysis of BCA at* 19 K, *based on the* 14 C *atoms of the annulene perimeter*

The parameters are referred to the Cartesian crystal frame a, b, c^*. Components of the translational **T** tensor are in $Å^2 \times 10^5$, those of the librational **L** tensor in deg^2. For the cross tensor **S** units are rad Å $\times 10^5$.

T			L		
445 (7)	18 (7)	−12 (8)	1.76 (21)	−0.34 (7)	−0.09 (7)
	347 (11)	13 (11)		0.76 (6)	−0.08 (4)
		435 (13)			0.64 (5)

S		
−4 (2)	15 (3)	−14 (3)
−9 (2)	1 (2)	3 (2)
9 (2)	−10 (2)	3 (2)

Eigenvalues of
T: 0.00454, 0.00432, 0.00341 $Å^2$
L: 1.87, 0.75, 0.54 deg^2
Goodness-of-fit: 2.21
wR^*: 0.051, 0.041

* The quantity wR is defined as $[\sum w(\Delta U_{ij})^2 / \sum w(U_{ij})^2]^{1/2}$ with the weights w taken as inversely proportional to the variance of U_{ij}; the first value is for all $U_{ij}'s$, the second for diagonal $U_{ij}'s$ only.

3.1. *Molecular motions*

The U_{ij} values of BCA at 19 K are smaller than those at room temperature (Destro & Simonetta, 1977) by a factor of *ca* 7.6; their e.s.d.'s are reduced, on average, 5.3 times. The rigid-bond test (Hirshfeld, 1976) is virtually perfect: the largest single difference of the mean-square displacement amplitudes (m.s.d.a.) of two bonded atoms in the direction of the bond is 5.3×10^{-4} Å^2 (for the C1—C2 bond), and the r.m.s. difference amounts to 1.8×10^{-4} Å^2. These values indicate that the data and the multipole model are both of very high quality.

A rigid-body **TLS** analysis (Schomaker & Trueblood, 1968; Dunitz, Schomaker & Trueblood, 1988) of the 18 non-H atoms gives a rather poor fit to the experimental a.d.p.'s, with calculated U_{ij} terms differing from observed by, on average, 3.5 e.s.d.'s. The matrix of the differences of observed m.s.d.a.'s for all 153 intramolecular pairs of heavy atoms of BCA clearly shows that the motion of the two O atoms and that of the remaining 16 C atoms are rather uncorrelated. Exclusion of the two O atoms from the **TLS** treatment yields a considerably better agreement (2.0 e.s.d.), and the same result is obtained if only the 14 C atoms of the annulene perimeter are included in the calculations. In both cases the matrix of the $\Delta_{M.S.D.A.}$ shows an average difference of 2×10^{-4} Å^2, and a r.m.s. Δ of 3×10^{-4} Å^2 (these two quantities were 4×10^{-4} and 7×10^{-4} Å^2, respectively, in the first analysis). Summaries of the three motional analyses have been deposited, while Table 5 gives the results for the third, smaller model. It is seen that the major components of the motion at 19 K appear to be translational in character, presumably lattice modes, with r.m.s. amplitudes 0.06–0.07 Å in the three crystal directions *a*, *b* and *c**. Irrespective of the number of atoms assumed to form a rigid body, the effects of the librational motion on bond lengths are less than 0.001 Å. Indeed, corrections to intramolecular distances range between 4 and 8×10^{-4} Å when **L** originates from the treatment of all 18 non-H atoms, and reduce to 3–6×10^{-4} Å for the model based on the 14 C atoms of the anthracene skeleton. It is worth mentioning that for the latter model the lengths of principal axes of the **L** tensor were 22, 11 and 5 deg^2 at room temperature, with corresponding corrections to the interatomic distances in the range 0.004–0.007 Å.

3.2. *The molecular geometry*

The molecular dimensions of BCA at 19 K are given in Figs. 1 and 2; Table 6 reports some interatomic distances of interest and Table 7 presents a comparison of *mm*2-averaged bond distances, as presently determined, both with those obtained experimentally at room temperature (Destro & Simonetta, 1977) and calculated by *ab initio* methods for an isolated molecule (Barzaghi, 1994) with geometry optimization at both the 6-31G* level and with second-order Møller–Plesset correlated wavefunctions (*MP*2/6-31G*). The following topics and features appear particularly worthy of note:

(1) The 'polarized H' facility of *VALRAY* has been really effective in determining the positional parameters of the H atoms: the resulting average C—H bond length for BCA, 1.089 (7) Å, is just slightly longer than the

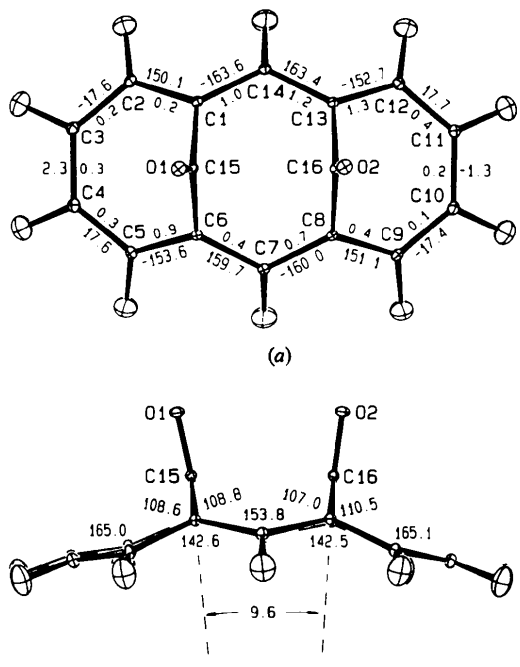

Fig. 1. Atomic numbering of BCA, with the molecule viewed along two principal axes of inertia. (*a*) Torsion angles (°) along the annulene perimeter (outwards), and absolute values of the differences (inwards) with respect to the room-temperature results. (*b*) Dihedral angles (°) between least-squares planes. Formal e.s.d.'s for all reported angles are < 0.1°. H atoms were numbered as for the C atoms to which they are bonded. The thermal ellipsoids are all drawn (H atoms on scale) for 50% probabilities.

mean value, 1.083 (11) Å, reported by Allen *et al.* (1987) for 218 neutron diffraction determinations of the C_{arom}—H bond distance.

(2) If we arbitrarily assume that all remaining systematic errors not accounted for in this experiment may amount to *ca* three times the estimated σ's from the least-squares refinement (Hamilton, 1969), the largest uncertainties for the BCA geometry are of 0.0015 Å in atomic distances and 0.1° in bond angles, when non-H atoms are implied.

(3) The values of the 14 ∠CCC angles along the annulene perimeter are all narrower, at 19 K, than those resulting from the 290 K investigation, with differences in the range 0.1–0.8° (average of the 14 Δ's = 0.47°). By contrast, the 8 ∠CCC bridgehead angles appear all wider, by 0.2–0.6° (average difference 0.34°), at lower T than room temperature, and scarcely significant are the differences, all within ±0.1°, for the four ∠CCO and the two bridging ∠CCC angles (*i.e.* C1—C15—C6 and C8—C16—C13). This situation is markedly different with respect to that observed for L-alanine, where the six bond angles involving non-H atoms, as measured in our 23 K experiment (Destro, Marsh & Bianchi, 1988), do not differ by more than 0.14° from those determined by neutron diffraction at 298 K (Lehmann, Koetzle & Hamilton, 1972). Such good agreement was not unexpected, since, as we noticed, neither librational nor electron polarization effects should have significant influence on the bond angles of that highly hydrogen-bonded amino acid. In conjunction with the observation (see Table 7) that room-temperature bond lengths of BCA, even when corrected for thermal motion, are still in rather poor agreement with the 19 K values, the systematic differences in bond angles noted above illustrate well, in our opinion, that proper modeling of the molecular motions is more demanding at room temperature than at 19 K.

(4) Strictly related to the previous point is the different classification of annulene C—C bond types that one

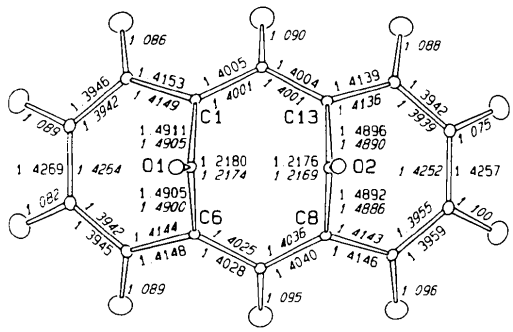

(*a*)

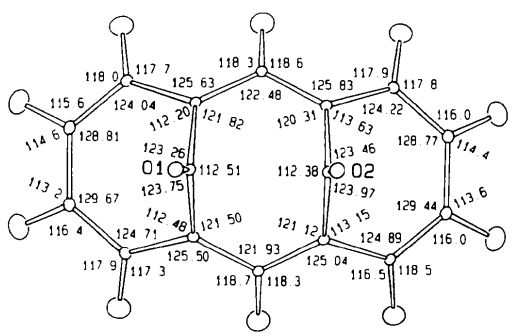

(*b*)

Fig. 2. Bond distances and angles of BCA at 19 K. (*a*) Bond lengths (Å), uncorrected (italics) and corrected for thermal motion. E.s.d.'s are ≤ 0.0005 Å for all bonds between non-H atoms, and 0.006–0.007 Å for C—H bonds. (*b*) Bond angles (°); e.s.d.'s are ≤ 0.03° for ∠C—C—C and ∠C—C—O angles, and in the range 0.3–0.4° for ∠C—C—H angles.

Table 6. *Intra- and intermolecular distances* (Å) *of interest for BCA at* 19 K

(*a*) Intramolecular distances (Å)

C1···C6	2.4784 (5)	C15···C16	2.5933 (5)
C8···C13	2.4740 (5)	O1···O2	3.0203 (6)

(*b*) Intermolecular contacts* (Å)

C5···O2	$\frac{1}{2}+x, \frac{1}{2}-y, -\frac{1}{2}+z$	3.1503 (5)
C13···C14	$1-x, -y, 1-z$	3.2675 (5)
C14···C14	$1-x, -y, 1-z$	3.1992 (6)
C9···H14	$\frac{1}{2}-x, \frac{1}{2}+y, \frac{1}{2}-z$	2.673 (7)
C10···H5	$-\frac{1}{2}+x, \frac{1}{2}-y, \frac{1}{2}+z$	2.887 (7)
C10···H14	$\frac{1}{2}-x, \frac{1}{2}+y, \frac{1}{2}-z$	2.877 (7)
O1···H2	$\frac{3}{2}-x, \frac{1}{2}+y, \frac{1}{2}-z$	2.596 (7)
O1···H7	$\frac{1}{2}+x, \frac{1}{2}-y, \frac{1}{2}+z$	2.601 (7)
O1···H9	$\frac{1}{2}+x, \frac{1}{2}-y, \frac{1}{2}+z$	2.451 (7)
O1···H10	$1+x, +y, +z$	2.686 (7)
O1···H11	$1+x, +y, +z$	2.589 (7)
O2···H3	$\frac{3}{2}-x, \frac{1}{2}+y, \frac{1}{2}-z$	2.599 (7)
O2···H9	$\frac{1}{2}+x, \frac{1}{2}-y, \frac{1}{2}+z$	2.428 (7)
H9···H14	$\frac{1}{2}-x, \frac{1}{2}+y, \frac{1}{2}-z$	2.279 (9)

* All distances smaller than the sum of the van der Waals radii, $r_C = 1.7$, $r_O = 1.5$ and $r_H = 1.2$ Å, are listed.

Table 7. *Comparison of interatomic distances* (Å) *in BCA, assuming mm2 symmetry*

Distance†	Experimental		Theoretical	
	290 K	19 K	6-31G*	MP2/6-31G*
C1—C2	1.410 (2)	1.4143 (5)		
	1.414	1.4147	1.413	1.411
C2—C3	1.379 (4)	1.3944 (7)		
	1.384	1.3948	1.372	1.395
C3—C4	1.409 (1)	1.4258 (8)		
	1.416	1.4263	1.424	1.421
C14—C1	1.393 (1)	1.4016 (18)		
	1.397	1.4019	1.390	1.400
C1—C15	1.487 (1)	1.4895 (9)		
	1.492	1.4901	1.489	1.491
C15—O1	1.208 (1)	1.2172 (4)		
	1.213	1.2178	1.184	1.225
C1···C6	2.471 (2)	2.4762 (31)		
	2.481	2.4772	2.441	2.473
C15···C16	2.591 (2)	2.5933 (5)		
	2.597	2.5938	2.646	2.579

† For the experimental distances, values are uncorrected (above) and corrected (below) for thermal motion. The e.s.d.'s (in parentheses) refer to the observed scatter of values contributing to the average in *mm2* symmetry.

would infer from the two experimental compilations of Table 7: there are four types of C—C bonds along the anthracene perimeter, according to the 19 K determination, but only three in the 290 K description, since at room temperature the C1—C2 bond length is not significantly different from the C3—C4 bond distance. Concomitantly, deviation from the *mm*2 symmetry for bond lengths is more marked at 19 than at 290 K. At the lower temperature the central portion of the annulene skeleton (see Fig. 2*a*) shows a top half – across the 'mirror' plane through the long molecular axis – significantly different from the bottom, with the C1—C14 and C13—C14 bonds much shorter than the C6—C7 and C7—C8 bonds. These differences are paralleled by different deviations from the theoretical value of 180° for the corresponding torsion angles (see the top of Fig. 1), such a reference value being obviously valid for a perfectly planar annulene system. It seems rather easy to consider these torsions being sensitive to crystal forces and, in turn, causing the bond lengths to respond to the variations in π-overlap.

(5) The largest differences (between 290 and 19 K values) for torsion angles along the annulene perimeter (Fig. 1) occur at angles involving atoms for which rather short C···C or C···O intermolecular contacts are observed (Table 6); the shortening of these distances on cooling amounts to *ca* 0.055 Å. On the other hand, the displacement of the two O atoms from their corresponding bridge-carbon planes are maintained greatly different from one another, and yet each is similar to that observed at room temperature: atom O1 deviates from the plane defined by atoms C1, C6 and C15 by 0.137 Å (*versus* 0.132 Å at 290 K), and O2 is displaced by 0.087 Å (*versus* 0.086 Å at 290 K) from the plane of atoms C8, C13 and C16. It appears that repulsive interactions between the two carbonyl groups and the resulting bending of the O atoms in a direction away from the center of the annulene system were already well described by the room-temperature experiment. It also appears that packing interactions involving the O atoms, mainly O···H interactions, play essentially the same role at the two temperatures, since the difference in the bending of the two carbonyl groups, 0.05 Å, is almost unaffected by the cooling.

(6) A detailed comparison between experiment and theory is in preparation (Barzaghi, Merati & Destro, 1995). We simply note here that *ab initio* values for the bond lengths (Table 7) are in much closer agreement with the experimental ones when the Møller–Plesset procedure is applied – a level of accuracy in computational work that is seldom attained for relatively large molecules.

3.3. *The topological analysis of* ρ_{exp}

According to Bader's quantum theory of atoms in molecules (*QTAM*; Bader, 1990*a*), a rigorous description of chemical bonds, and in general of atomic interactions, can be obtained through the study of the topology of the total charge density. As for any scalar field, the essential topological features of $\rho(\mathbf{r})$ are summarized by the properties of its critical points $\mathbf{r}_c$, sites where $\nabla\rho = 0$. The number and signs of the principal curvatures of ρ at $\mathbf{r}_c$ are used to define two integer numbers (m, n), named rank and signature, respectively, of the critical point. The rank m is the number of nonvanishing eigenvalues of the Hessian matrix of ρ at $\mathbf{r}_c$, and the signature n is the algebraic sum of the signs of the principal curvatures – the eigenvalues – of ρ at $\mathbf{r}_c$. Thus, atomic positions are all $(3, -3)$ critical points of ρ. Two atomic positions are said to be involved in a bonding interaction if in $\rho(\mathbf{r})$ there is a line, linking the nuclei, along which the charge density is at a maximum with respect to any lateral displacement. This line of maximum charge density is known as a *bond path*, and the $(3,-1)$ critical point occuring on it (a saddle point) a *bond critical point* (b.c.p).

A summary of concepts and definitions of these and other quantities used in the topological analysis of $\rho(\mathbf{r})$ has been given recently by Bader (1990*b*); descriptions particularly devoted to experimental charge densities can also be found in recent literature (*e.g.* Craven & Stewart, 1990; Stewart, 1991; Gatti, Bianchi, Destro & Merati, 1992).

Thanks to the analytical representation of the electron density afforded by the multipole expansion (in our case equation 10 of Stewart, 1976), the gradient and Hessian of $\rho(\mathbf{r})$ can be evaluated at any desired point in the crystal with a direct space lattice sum (Stewart & Spackman, 1983). A Newton–Raphson procedure is adopted in *VALRAY* to locate the critical points, starting from a suitable initial guess for their positions.

All expected b.c.p.'s for the 20 C—C and C—O bonds, as well as those of the ten C—H bonds of BCA, were easily located; their properties are listed in Table 8. In view of the substantial identity, in chemical terms, of the ten C—H bonds, the properties of their b.c.p's have been reported as averages. Table 8 also includes the $(3, -1)$ critical points for the seven O···H intermolecular contacts of Table 6. The positions of the b.c.p.'s for the bonds of one of the two carbonyl bridges of BCA are visualized in the maps of Fig. 3, while Fig. 4 illustrates the features of ρ and $\nabla^2\rho$ at the b.c.p.'s of two C—H bonds and two O···H interactions.

Inspection of Table 8 reveals that the b.c.p.'s of the two C—O bonds are much closer to the C atoms (at 36% of the bond distance) than to the O atoms, and the ten b.c.p.'s of the C—H bonds are found, on average, at 63% of the bond distance towards the H atoms. All 18 b.c.p.'s of the C—C bonds are instead very close to the bond midpoints, with a maximum shift of 0.032 Å (*ca* 2% of the bond distance) for the C1—C15 bond. This is the expected behavior for non-polar C—C bond paths. As in the present experimental case, theoretically investigated C—C bonds (*e.g.* Bader & Essén, 1984)

show values of ρ_{bcp} systematically decreasing with increasing length of the bond, *i.e.* with an increasing single bond character (compare here the properties of the b.c.p.'s for the 14 bonds of the annulene perimeter with those of the four C—C bonds of the bridges).

All covalent bonds of BCA are characterized by negative values of the Laplacian of ρ at the b.c.p.'s, a feature that agrees with *ab initio* results of good quality, *e.g.* 6-31G** calculations [see, for example, the theoretical values of L-alanine (Gatti, Bianchi, Destro & Merati, 1992)]. It is worth mentioning that our multipolar representation of the charge density is accompanied by rather low values of the e.s.d.'s of ρ at the bond critical points, better than 1% for all covalent bonds. Even the Laplacian of ρ, a quantity more demanding on the quality of the experiment, has been obtained for BCA with a relatively high precision, the largest e.s.d. for the $\nabla^2\rho_{bcp}$ of Table 8 being less than 4% of the Laplacian for all covalent bonds. Larger relative uncertainties are associated with ρ and $\nabla^2\rho$ at the (3, −1) critical points of the intermolecular CH···O interactions, where, however, values as small as 0.04 e Å^{-3} for ρ an 0.54 e Å^{-5} for $\nabla^2\rho$ appear to be still determined with high precision, such values being 20–30 times larger than their e.s.d.'s.

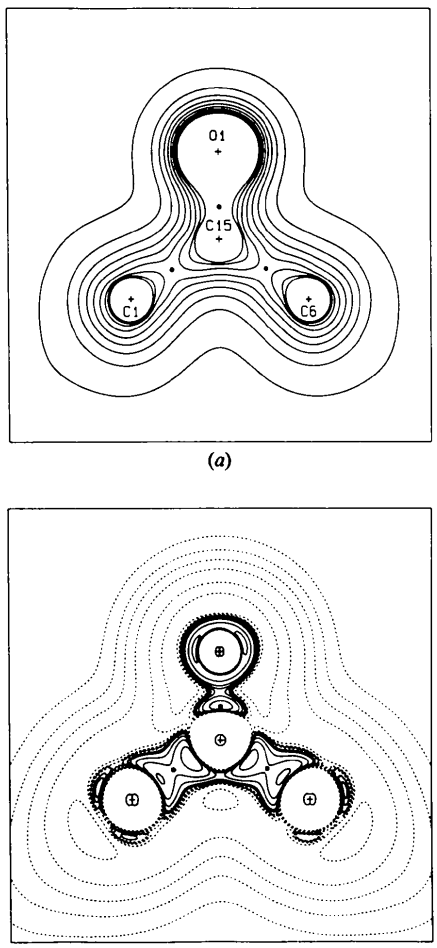

(*a*)

(*b*)

Fig. 3. Contour maps (6 × 6 Å) of (*a*) the experimental ρ_{exp} and (*b*) its negative Laplacian $-\nabla^2\rho_{exp}$ in the plane defined by atoms C1, C6 and O1. C15 is displaced 0.055 Å from the plane. Contour levels for ρ are at intervals of 0.3 e Å^{-3}, from a minimum value (outermost contour) of 0.1 e Å^{-3} to a maximum of 2.50 e Å^{-3}. The Laplacian is plotted in units of e Å^{-5}; the short dashed lines describe the positive region of $\nabla^2\rho_{exp}$, at values 0.2, 0.5, 1.0, 2.0, 5.0 and 10.0. The zero level is omitted, while negative values of Laplacian, indicating charge concentration, are denoted by solid lines at 1.0, 2.0, 5.0, 10.0, 20.0, 50.0 and 90.0 e Å^{-5}. The latter value is used only for the two small contours revealing the lone-pair charge concentration on the O atom. The three solid circles mark the positions, projected onto the plane, of the b.c.p.'s, which are all three off the plane by *ca* 0.037 Å, on the same side as C15.

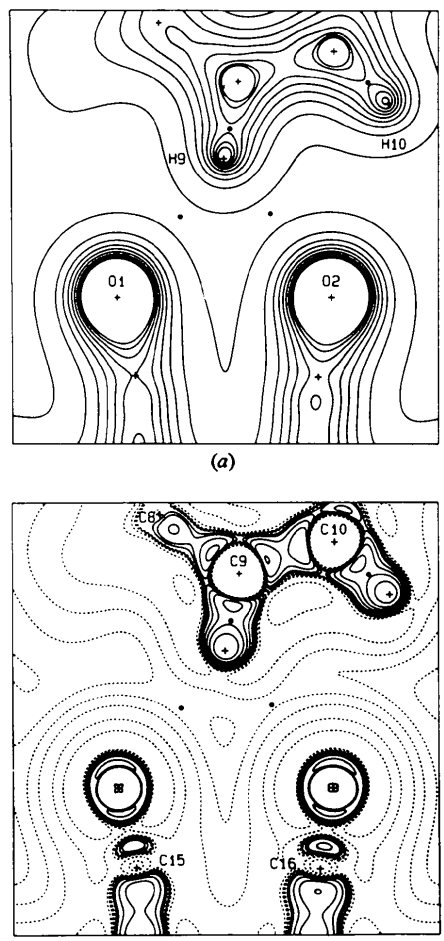

(*a*)

(*b*)

Fig. 4. As in Fig. 3 for the plane defined by O1, O2 and H9, the latter at $\frac{1}{2}+x, \frac{1}{2}-y, \frac{1}{2}+z$. In the negative region of the Laplacian (continuous lines) the highest level here is 50 (instead of 90) e Å^{-5}. Distances (Å) from the plane for the other atoms labelled in the figure are: C8, 0.506; C9, 0.205; C10, 0.239; H10, −0.110; C15, −0.448; C16, −0.432. The two (3, −1) critical points relative to the C9—H9···O interactions, marked by the solid circles near the center of the maps, are displaced from the plane by −0.032 and −0.006 Å, the closer to the plane being that of H9···O2. The b.c.p. of the C9—H9 bond is 0.083 Å off the plane, that of the C10—H10 bond 0.025 Å.

Table 8. *Bond-critical-point (b.c.p.) properties* of BCA in the crystal state*

Bond ($X-Y$)	R† (Å)	R_x‡ (Å)	ρ_{bcp} §	$\nabla^2\rho_{bcp}$ ¶	λ_1	λ_2	λ_3	ε**
(*a*) Intramolecular bonds								
C1—C2	1.415	0.680	2.01 (1)	−13.9 (3)	−14.5	−12.7	13.3	0.15
C5—C6	1.414	0.704	2.04 (1)	−14.3 (2)	−14.8	−12.9	13.4	0.15
C8—C9	1.414	0.732	2.03 (1)	−14.7 (4)	−14.9	−13.0	13.2	0.15
C12—C13	1.414	0.680	2.03 (1)	−14.4 (4)	−14.8	−12.8	13.2	0.16
C2—C3	1.394	0.682	2.12 (1)	−15.4 (3)	−15.9	−13.1	13.6	0.21
C4—C5	1.394	0.683	2.08 (1)	−14.6 (3)	−15.4	−12.8	13.6	0.20
C9—C10	1.396	0.695	2.10 (1)	−15.1 (2)	−15.3	−13.7	13.9	0.11
C11—C12	1.394	0.685	2.09 (1)	−14.7 (3)	−15.4	−13.1	13.8	0.17
C3—C4	1.426	0.703	1.96 (1)	−13.0 (4)	−14.2	−12.3	13.5	0.15
C10—C11	1.425	0.706	1.98 (1)	−13.7 (3)	−14.5	−12.6	13.4	0.15
C1—C14	1.400	0.695	2.08 (1)	−14.5 (3)	−15.5	−12.7	13.7	0.22
C6—C7	1.402	0.724	2.09 (1)	−15.4 (3)	−15.7	−13.0	13.3	0.21
C7—C8	1.404	0.688	2.08 (1)	−15.3 (3)	−15.4	−13.2	13.3	0.17
C13—C14	1.400	0.719	2.10 (1)	−15.4 (4)	−15.8	−13.0	13.4	0.21
C1—C15	1.490	0.713	1.79 (1)	−11.3 (3)	−12.4	−12.0	13.1	0.03
C6—C15	1.490	0.730	1.82 (1)	−12.1 (4)	−12.8	−12.4	13.1	0.04
C8—C16	1.489	0.724	1.84 (1)	−12.4 (4)	−12.9	−12.7	13.1	0.02
C13—C16	1.489	0.721	1.82 (1)	−12.2 (3)	−12.7	−12.6	13.0	0.01
C15—O1	1.217	0.440	2.96 (3)	−27.9 (7)	−28.9	−25.0	25.9	0.16
C16—O2	1.217	0.442	3.00 (3)	−30.1 (11)	−29.5	−25.6	25.1	0.15
C15—C16	2.593	1.292	0.116 (3)	1.53 (1)	−0.14	−0.06	1.73	1.33
⟨C—H⟩††	1.089	0.685	1.89 (3)	−18.1 (8)	−18.1	−17.5	17.5	0.03
(*b*) Intermolecular —CH···O contacts‡‡								
O1···H2	2.596	1.516	0.043 (2)	0.67 (2)	−0.14	−0.11	0.92	0.27
O1···H7	2.601	1.491	0.041 (2)	0.58 (1)	−0.13	−0.12	0.83	0.08
O1···H9	2.451	1.425	0.060 (3)	0.74 (2)	−0.22	−0.20	1.16	0.10
O1···H10	2.686	1.531	0.040 (2)	0.54 (2)	−0.11	−0.10	0.74	0.10
O1···H11	2.589	1.472	0.050 (2)	0.67 (2)	−0.16	−0.14	0.97	0.14
O2···H3	2.599	1.512	0.043 (2)	0.56 (1)	−0.15	−0.14	0.85	0.07
O2···H9	2.428	1.412	0.062 (3)	0.91 (2)	−0.22	−0.17	1.30	0.29

* For the total charge density and its Laplacian e.s.d.'s are given in parentheses. The evaluation of the e.s.d. of $\nabla^2\rho$ was made by a locally written code, added to the version of *VALRAY* in use in our laboratory.

† Experimental bond length, rounded up to the third decimal digit, uncorrected for thermal motion.

‡ Distance between the b.c.p. and the atom X forming the $X-Y$ bond.

§ Electron density at the bond critical point in e Å^{-3}.

¶ Laplacian of ρ_{bcp} in e Å^{-5}, related to the principal values of the curvature (λ_i's) by: $\nabla^2\rho = \lambda_1 + \lambda_2 + \lambda_3$.

** Bond ellipticity, defined as $\varepsilon = \lambda_1/\lambda_2 - 1$.

†† Average values for the ten C—H bonds with sample e.s.d.'s.

‡‡ See Table 6 for the symmetry codes of the H atoms.

Table 9. *Topological properties* at the four* (3,1) *critical points of* ρ_{exp} *in BCA crystals*

Ring†	x	y	z	ρ_{rcp}	$\nabla^2\rho_{rcp}$	λ_1	λ_2	λ_3
7*mR*1	0.7136	0.0436	0.1535	0.093 (3)	1.77 (1)	−0.11	0.63	1.25
7*mR*2	0.2445	0.1363	0.2784	0.092 (3)	1.74 (1)	−0.10	0.71	1.13
5*mR*3	0.5191	0.1480	0.2626	0.115 (3)	1.54 (1)	−0.25	0.08	1.71
5*mR*4	0.5203	0.1158	0.2987	0.114 (3)	1.54 (1)	−0.24	0.09	1.70

* For each of the ring critical points (r.c.p.) fractional coordinates, ρ (e Å^{-3}), Laplacian of $\rho(\nabla^2\rho$, e Å^{-5}) and principal curvatures λ's (e Å^{-5}) are reported.

† 7*mR*1 = (seven-membered) ring no. 1: C1, C2, C3, C4, C5, C6 and C15; 7*mR*2 = (seven-membered) ring no. 2: C8, C9, C10, C11, C12, C13 and C16; 5*mR*3 = (five-membered) ring no. 3: C15, C6, C7, C8 and C16; 5*mR*4 = (five-membered) ring no. 4: C15, C1, C14, C13 and C16.

Perhaps the most unexpected feature revealed by the topological analysis of the BCA charge density is the presence of a (3, −1) critical point (see Fig. 5 and Table 8) almost exactly midway between the two bridge atoms C15 and C16, possibly implying the existence of a weak bond due to steric interaction. As pointed out by Cioslowski, who has recently investigated by *ab initio* calculations several cases of unusual interatomic interactions (Cioslowski, Mixon & Edwards, 1991; Cioslowski & Mixon, 1992), these weak bonds challenge the traditional ideas about bonding in organic molecules. In the present paper we confine ourselves to the following two observations:

(1) No critical point of the (3, −1) type is found along, or in proximity of, the lines connecting C1 to C6, or C8 to C13, these two transannular distances being shorter (see Table 6), by more than 0.1 Å, than the C15—C16 separation; the occurrence of the critical point here under

discussion is therefore not simply related to a particularly short C···C contact.

(2) In the usual description of the BCA molecule, its central portion is obviously considered an eight-membered ring. By contrast, the existence of a bond – although weak – between the two bridging C atoms would imply the description of the annulene system of BCA as comprising, besides the two lateral seven-membered rings, two five-membered rings, one formed by atoms C15, C6, C7, C8 and C16, and the other by C15, C1, C14, C13 and C16. According to Bader's topological theory, a (3, +1) critical point must be found in the interior of each ring, if any is present in a molecular structure. For BCA, four well defined (3, +1) critical points were found, two associated with the seven-membered rings, and the other two, symmetrically located with respect to the pseudomirror plane through the long molecular axis, associated with the five-membered rings. The properties of the four ring critical points are summarized in Table 9. The nature of the C15···C16 interaction revealed by the presence of the (3, −1) critical point – be it, as mentioned above, a weak bond, or a nonbonding repulsive interaction, if not an artifact – is under study by *ab initio* methods. However, we cannot ignore that thermal decomposition of BCA occurs to 30% as decarbonylation to anthracene and carbon monoxide, but 70% of the annulene is deoxygenated to give, *via* the 1,2-dioxetane obtained by connecting with chemical bonds atoms O1–O2 and C15–C16, the pyrene isomer dicyclohepta[*cd*,*gh*]pentalene, alternatively named azuleno[2,1,8-*ija*]azulene (Vogel *et al.*, 1984). The latter is a planar, centrosymmetric molecule, whose structure, studied by X-ray diffraction (Vogel, Wieland, Schmalstieg & Lex, 1984), comprises indeed two seven- and two five-membered rings.

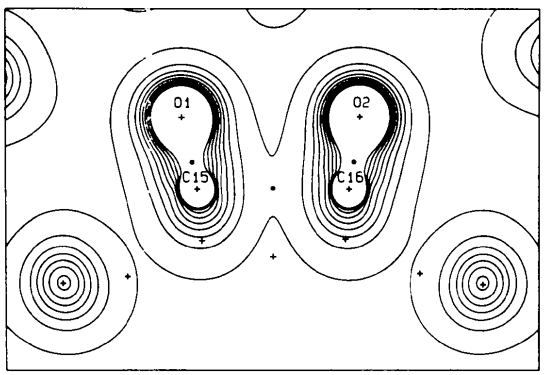

(*a*)

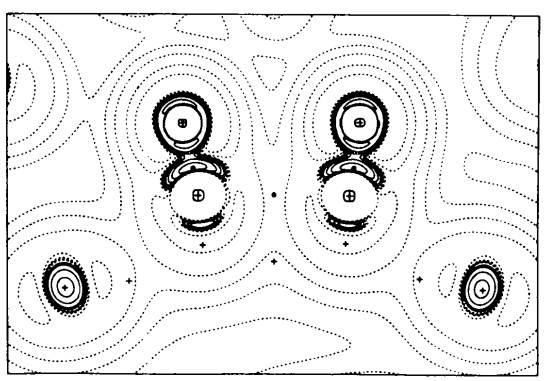

(*b*)

Fig. 5. (*a*) Map of ρ_{exp} (e Å^{-3}) in the plane of the two carbonyl groups of BCA. The plane is defined by atoms C15 and C16, and the midpoint between atoms O1 and O2. Since the torsion angle O1—C15—C16—O2 amounts to −1.26 (3)°, the two O atoms are displaced by equal amounts (0.013 Å) on opposite sides of the plane. The two b.c.p.'s (solid circles) of the C—O bonds are virtually on the plane (displacements < 0.007 Å), while the third (3, −1) critical point reported in the figure, relative to the C15···C16 interaction, is displaced from the plane by 0.010 Å. Its projection onto the plane coincides with the center of the map. The seven nonlabeled crosses represent projections onto the plane for half the C atoms of the longitudinal profile of the anthracene skeleton (as in Fig. 1*b*). The two peaks of 1.9 e Å^{-3} at the lower corners of the map refer to the midpoints of the C3—C4 (left) and C10—C11 (right) bonds. (*b*) Corresponding contour maps of $-\nabla^2\rho_{exp}$. Contour levels in both maps as in Fig. 4.

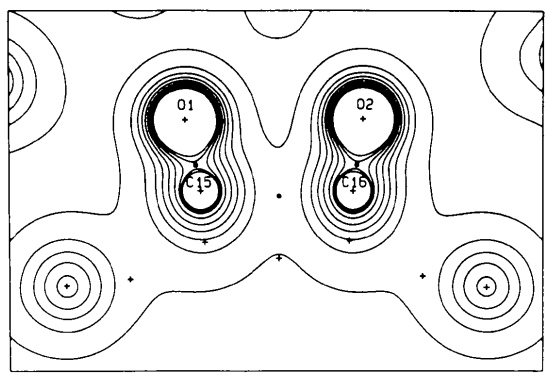

(*a*)

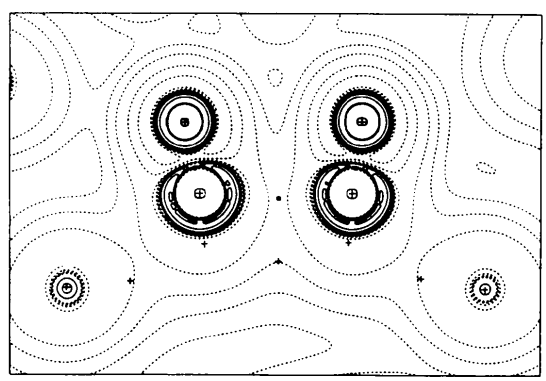

(*b*)

Fig. 6. As in Fig. 5, with ρ and its Laplacian obtained from the IAM (= spherical atom) model.

4. Concluding remarks

The present work confirms that stated during our study of L-alanine, *i.e.* that from an extensive set of X-ray diffraction intensities accurately measured at $T < 30\,K$ and properly corrected, the molecular geometry can be recovered in all details at a very high degree of confidence. Analysis of the X-ray data by a multipole model is an essential part of the procedure, since scattering by electrons in the valence shell is not adequately represented by the spherically symmetric atom scattering factors normally used. In the case of BCA, an illustration of the differences in interpreting the experimental data with a multipole model or by the spherical independent atom model (IAM) is given by a simple visual comparison of Fig. 6 with Fig. 5.

The merits of the topological analysis of ρ_{exp}, as a valuable tool to properly describe the molecular structure, have been documented. Although the occurrence of chemically unexpected features, as here the (3, −1) critical point for the C15···C16 separation, will happen rather seldom, we believe that the determination of the properties of ρ_{exp} at its critical points is at present the most adequate procedure to fully and quantitatively characterize chemical bonds in crystals.

We are grateful to Professor A. Gavezzotti for his valuable contribution in the early stages of low-T data collection and processing, Dr R. Bianchi for preliminary computations with the multipole models, Dr M. Barzaghi for calculation of the *ab initio* geometries, and Drs P. Roversi and R. Soave for their great help in the preparation of the manuscript. Profitable discussions with Dr R. E. Marsh on the treatment of intensity data, and with Professor R. F. Stewart on the best usage of the set of *VALRAY* programs he supplied us, are also acknowledged.

References

ALLEN, F. H., KENNARD, O., WATSON, D. G., BRAMMER, L., ORPEN, A. G. & TAYLOR, R. (1987). *J. Chem. Soc. Perkin Trans.* 2, S1–S19.
ARTIOLI, G. (1994). Personal communication.
BADER, R. F. W. (1990*a*) *Atoms in Molecules – A Quantum Theory*. Oxford Univ. Press.
BADER, R. F. W. (1990*b*). *Trans. Am. Cryst. Assoc.* **26**, 1–21.
BADER, R. F. W. & ESSÉN, H. (1984). *J. Chem. Phys.* **80**, 1943–1960.
BALCI, M., SCHALENBACH, R. & VOGEL, E. (1981). *Angew. Chem. Int. Ed. Engl.* **20**, 809–811.
BARZAGHI, M. (1994). Personal communication.
BARZAGHI, M., MERATI, F. & DESTRO, R. (1995). In preparation.
BECKER, P. J. & COPPENS, P. (1974). *Acta Cryst.* A**30**, 129–147.
CIOSLOWSKI, J. & MIXON, S. T. (1992). *J. Am. Chem. Soc.* **114**, 4382–4387.
CIOSLOWSKI, J., MIXON, S. T. & EDWARDS, W. D. (1991). *J. Am. Chem. Soc.* **113**, 1083–1085.
CLEMENTI, E. (1965). Tables of atomic functions, supplement to *IBM J. Res. Dev.* **9**(2).
COCHRAN, W. (1953). *Acta Cryst.* **6**, 260–268.
CRAVEN, B. M. & STEWART, R. F. (1990). *Trans. Am. Cryst. Assoc.* **26**, 41–54.
CRUICKSHANK, D. W. J. (1949). *Acta Cryst.* **2**, 65–82.
DESTRO, R. (1988). *Aust. J. Phys.* **41**, 503–510.
DESTRO, R. & MARSH, R. E. (1987). *Acta Cryst.* A**43**, 711–718.
DESTRO, R. & MARSH, R. E. (1993). *Acta Cryst.* A**49**, 183–190.
DESTRO, R. & MERATI, F. (1993). *Z. Naturforsch. Teil A*, **48**, 99–104.
DESTRO, R. & SIMONETTA, M. (1977). *Acta Cryst.* B**33**, 3219–3221.
DESTRO, R., BIANCHI, R., GATTI, C. & MERATI, F. (1991). *Chem. Phys. Lett.* **186**, 47–52.
DESTRO, R., MARSH, R. E. & BIANCHI, R. (1988). *J. Phys. Chem.* **92**, 966–973.
DUNITZ, J. D., SCHOMAKER, V. & TRUEBLOOD, K. N. (1988). *J. Phys. Chem.* **92**, 856–867.
GATTI, C., BIANCHI, R., DESTRO, R. & MERATI, F. (1992). *J. Mol. Struct. (Theochem.)* **255**, 409–433.
HAMILTON, W. C. (1969). *Acta Cryst.* A**25**, 194–206.
HARKEMA, S., DAM, J., VAN HUMMEL, G. J. & REUVERS, A. J. (1980). *Acta Cryst.* A**36**, 433–435.
HEHRE, W. J., STEWART, R. F. & POPLE, J. A. (1969). *J. Chem. Phys.* **51**, 2657–2664.
HIRSHFELD, F. L. (1976). *Acta Cryst.* A**32**, 239–244.
HIRSHFELD, F. L. (1990). Personal communication.
LEHMANN, M. S., KOETZLE, T. F. & HAMILTON, W. C. (1972). *J. Am. Chem. Soc.* **94**, 2657–2660.
MARSH, R. E. (1958). *Acta Cryst.* **11**, 654–663.
SAMSON, S., GOLDISH, E. & DICK, C. J. (1980). *J. Appl. Cryst.* **13**, 425–432.
SCHOMAKER, V. & MARSH, R. E. (1983). *Acta Cryst.* A**39**, 819–820.
SCHOMAKER, V. & TRUEBLOOD, K. N. (1968). *Acta Cryst.* B**24**, 63–76.
SPACKMAN, M. A. (1992). *Chem. Rev.* **92**, 1769–1797.
STEWART, R. F. (1968). *J. Chem. Phys.* **48**, 4882–4889.
STEWART, R. F. (1972). *J. Chem. Phys.* **57**, 1664–1668.
STEWART, R. F. (1976). *Acta Cryst.* A**32**, 565–574.
STEWART, R. F. (1991). In *The Application of Charge Density Research to Chemistry and Drug Design*, NATO-ASI Series B, Vol. 250, pp. 63–101. New York: Plenum Press.
STEWART, R. F. & SPACKMAN, M. A. (1983). *VALRAY*. Carnegie Mellon Univ., Pittsburgh, PA.
STEWART, R. F., BENTLEY, J. J. & GOODMAN, B. (1975). *J. Chem. Phys.* **63**, 3786–3793.
VOGEL, E., MARKOWITZ, G., SCHMALSTIEG, L., ITÔ, S., BREUCKMANN, R. & ROTH, W. R. (1984). *Angew. Chem. Int. Ed. Engl.* **23**, 719–720.
VOGEL, E., WIELAND, H., SCHMALSTIEG, L. & LEX, J. (1984). *Angew. Chem. Int. Ed. Engl.* **23**, 717–719.